crystals

MDPI

Article

Effect of Ceria Doping on the Mechanical Properties and Phase Stability of Partially Samaria-Stabilized Zirconia Crystals

Mikhail Borik [1], Artem Chislov [1,2], Alexej Kulebyakin [1], Elena Lomonova [1], Filipp Milovich [2,3], Valentina Myzina [1], Vladimir Pankratov [4], Alexandr Poselennov [2], Polina Ryabochkina [5], Natalia Sidorova [5], Nataliya Tabachkova [1,2,*], Denis Zakharov [1,2] and Dmitry Kiselev [2]

1 Prokhorov General Physics Institute of the Russian Academy of Sciences, 38 Vavilov Str., 119991 Moscow, Russia; borik@lst.gpi.ru (M.B.); chislov.as@misis.ru (A.C.); kulebyakin@lst.gpi.ru (A.K.); lomonova@lst.gpi.ru (E.L.); vamyzina@lst.gpi.ru (V.M.); m1604564@edu.misis.ru (D.Z.)
2 Department of Materials Science of Semiconductors and Dielectrics, National University of Science and Technology (MISIS), 4 Leninskiy Prospekt, 119049 Moscow, Russia; milovich.fo@misis.ru (F.M.); m1603665@edu.misis.ru (A.P.); dm.kiselev@misis.ru (D.K.)
3 Department of Materials Science, Moscow Polytechnic University, Bolshaya Semyonovskaya Street, 38, 107023 Moscow, Russia
4 Institute of Solid State Physics, University of Latvia, 8 Kengaraga, LV-1063 Riga, Latvia; vladimirs.pankratovs@cfi.lu.lv
5 Institute of High Technologies and New Materials, Ogarev Mordovia State University, 68 Bolshevistskaya Str., 430005 Saransk, Russia; ryabochkina@freemail.mrsu.ru (P.R.); sidorova-n.v@mrsu.ru (N.S.)
* Correspondence: ntabachkova@misis.ru; Tel.: +7-(916)-647-19-54

Abstract: The effect of ceria doping of $(ZrO_2)_{1-x}(Sm_2O_3)_x$ crystals on their phase composition, microhardness and fracture toughness was studied. The $(ZrO_2)_{0.995-x}(Sm_2O_3)_x(CeO_2)_{0.005}$ crystals (where x = 0.032, 0.037 and 0.04) were grown using directional melt crystallization in a cold crucible. The mechanical properties, such as microhardness and fracture toughness, were explored using Vickers indentation. It was shown that the $(ZrO_2)_{0.995-x}(Sm_2O_3)_x(CeO_2)_{0.005}$ solid-solution crystals contained both Ce^{4+} and Ce^{3+} ions. Phase analysis data suggested that CeO_2 doping increased the tetragonality degree of the transformable t phase and reduced the tetragonality degree of the non-transformable t' phase as compared to the $(ZrO_2)_{1-x}(Sm_2O_3)_x$ crystals. As a result, the t→m phase transition triggered by the indentation-induced stress in the CeO_2-doped crystals was more intense and covered greater regions. CeO_2 doping of the solid solutions increased the fracture toughness of all the crystals studied, whereas the microhardness of the crystals changed only slightly. CeO_2 doping of the $(ZrO_2)_{1-x}(Sm_2O_3)_x$ solid solutions in the experimental concentration range did not improve the high-temperature phase stability of the crystals and did not prevent high-temperature degradation of their fracture toughness.

Keywords: Ce-Sm-PSZ; directional melt crystallization; solid solutions; fracture toughness; ZrO_2

Citation: Borik, M.; Chislov, A.; Kulebyakin, A.; Lomonova, E.; Milovich, F.; Myzina, V.; Pankratov, V.; Poselennov, A.; Ryabochkina, P.; Sidorova, N.; et al. Effect of Ceria Doping on the Mechanical Properties and Phase Stability of Partially Samaria-Stabilized Zirconia Crystals. *Crystals* **2024**, *14*, 736. https://doi.org/10.3390/cryst14080736

Academic Editors: Andrey Prokofiev, Xiaochun Li and Robert A. Jackson

Received: 10 July 2024
Revised: 30 July 2024
Accepted: 16 August 2024
Published: 19 August 2024

1. Introduction

Partially stabilized zirconia-based materials possess good mechanical properties and, therefore, a wide application range, including construction ceramics, wear-resistant bearings, heat protective coatings, oxygen-conducting solid-state electrolytes, biomedical devices, etc. [1–5].

The high strength of the abovementioned materials is primarily determined by the transformation strengthening mechanism [1,2,6]. Strengthening takes place as a result of a phase transition from the metastable tetragonal phase to the stable monoclinic one, the lattice parameters of which are greater than those of the tetragonal phase. The phase composition of zirconia-based solid solutions depends on the type and concentration of stabilizing oxides [7–9]. The most widely used stabilizing oxides are yttria and ceria. ZrO_2-based solid solutions partially stabilized with CeO_2 are of great interest due to their

high fracture toughness [2,10–13]. However, the strength parameters of those materials, such as microhardness, Young's modulus and flexure strength are inferior to those of yttria-stabilized zirconia-based materials.

Apart from yttrium, almost all trivalent rare-earth metal ions form zirconia-based solid solutions. Solid-state thermodynamic metastable tetragonal zirconia solutions, the compositions of which pertain to the (c + t) two-phase field of the phase diagram, are of greatest interest because of their good mechanical characteristics. The width of the (c + t) field changes depending on the stabilizing of the cation radius at a certain temperature. Smaller cations, e.g., yttrium or ytterbium, have wider tetragonal fields (up to ~2.5 mol.% R_2O_3) and narrow tetragonal (t + c) fields (2.5–7 mol.% R_2O_3) (R = rare-earth element). The t/(t + c) phase boundary shifts towards lower stabilizing oxide concentrations with an increase in the ionic radius of the stabilizing oxide, whereas the (t + c)/c boundary shifts towards higher stabilizing oxide contents [14,15]. Furthermore, stabilization of tetragonal solid solutions with larger-diameter cations entails a deeper phase decomposition and triggers the formation of the t and t' phases, the compositions of which are close to the t/(t + c) and (t + c)/c phase boundaries [16]. The proximity of the metastable t phase composition to the t/(c + t) phase boundary favors the stress-induced t→m phase transition and hence increases the transformability of the material. Comparison between the mechanical properties of the crystals, depending on the ionic radius of trivalent cation in the series RY^{3+} = 0.1019 nm < RGd^{3+} = 0.1053 nm < RSm^{3+} = 0.1074 nm, showed that the fracture toughness of the $(ZrO_2)_{1-x(}(R_2O_3)_x$ tetragonal crystals, where R = Y, Gd and Sm, increases with the ionic radius of the trivalent cation [17]. However, the fracture toughness of the synthesized partially stabilized zirconia decreases significantly if the material contains the monoclinic phase. Along with good mechanical parameters, of special importance is the long-term stability of these parameters under cycled loads and at elevated temperatures and humidity [18–21]. Optimizing of the mechanical properties of the materials and increasing their stability are achieved through co-doping with several oxides. There are a number of works dealing with yttria and ceria co-doping of zirconia and study of their parameters depending on the composition, grain structure and synthesis conditions [8,9,22]. However, there are but a few publications on co-doping with ceria and other rare-earth element oxides. YSZ co-doping with ceria and neodymia delivered good mechanical properties and, furthermore, provided for their preservation upon heat treatment [23]. One can expect that co-doping of ZrO_2-based solid solutions with ceria and rare-earth element oxides having greater cation radius than Y^{3+} will produce materials combining high strength and fracture toughness.

Earlier studies of $(ZrO_2)_{1-x}(Sm_2O_3)_x$ solid-solution crystals showed them to have high fracture toughness [24]. The aim of this work was to study the phase composition, microhardness and fracture toughness of $(ZrO_2)_{1-x}(Sm_2O_3)_x$ crystals doped with 0.5 mol.% CeO_2. The 0.5 mol.% ceria concentration was chosen based on the following reasons: On the one hand, cerium-containing ceramics having high fracture toughness typically have higher ceria concentrations. On the other hand, directional melt crystallization of high-ceria crystals causes ceria displacement from the crystallization front and eventually hinders the growth of homogeneous single crystals.

2. Materials and Methods

The $(ZrO_2)_{0.995-x}(Sm_2O_3)_x(CeO_2)_{0.005}$ crystals (where x = 0.032, 0.037 and 0.04) were grown using directional melt crystallization in a 100 mm diameter water-cooled crucible with direct high frequency heating. The melt was crystallized by moving the crucible out of the heating zone at a 10 mm/h. Melt crystallization starts upon melt cooling to the liquid's temperature. In this temperature range, multi-center crystal precipitation and growth occur, the latter being accompanied by a decrease in the number of the crystals since growth is a competitive process which depends on growth rate during directional melt crystallization. As one moves from the crystallization front, the grown crystals cool down to the cubic-to-tetragonal transition temperature (2300–2200 °C depending on stabilizing

oxide concentration) and remain single-phase and cubic. Further cooling causes a cubic-to-tetragonal transition.

The phase composition of the crystals was studied using X-ray diffraction on a Bruker D8 diffractometer. Melt-crystallization-grown $(ZrO_2)_{0.995-x}(Sm_2O_3)_x(CeO_2)_{0.005}$ crystals do not have preferential crystallographic growth orientation, and therefore each crystal was preliminarily oriented relative to specific crystallographic directions. The crystals were then cut into wafers perpendicular to the <001> direction. The diffraction patterns of the wafers cut from the crystals exhibited different-order reflections from the crystallographic plane parallel to the cut. Twinning in the crystals produced simultaneous different-order reflections from the {001} and {110} planes in wafers cut perpendicularly to the <001> direction.

Local-phase analysis in the vicinity of indentations was conducted using Raman spectroscopy under a Renishaw inVia microscope/spectrometer. Combination scattering spectra were recorded in a backscattering setup in mapping mode along the <100> and <110> crystallographic directions in 532 nm excited laser radiation. A 20× objective was used for spectrum recording, the laser spot diameter was 1 μm, and the exposure time was 5 s.

The structure of the crystals was studied using transmission electron microscopy (TEM) under a JEM-2100 microscope (JEOL, Tokyo, Japan) at a 200 kV acceleration voltage. For this, 3 mm thick wafers were cut ultrasonically. The as-cut specimens were ground to a thickness of ~100 μm; then, a cavity to a thickness of ~25 μm was made in the specimen center. The final thinning stage was Ar ion beam etching. The morphology and sizes of the twins in the $(ZrO_2)_{0.995-x}(Sm_2O_3)_x(CeO_2)_{0.005}$ tetragonal crystals were studied in diffraction contrast mode.

The microhardness and fracture toughness of the crystals were compared by indentation in the {100} plane for different specimen rotation angles in the specimen plane. The tests were conducted with a DM 8 B AUTO microhardness tester (Vicker's indenter, maximum load 20 N) and a Wolpert Hardness Tester 930 with a minimum load of 50 N. The microhardness and fracture toughness were measured at 5 and 200 N loads, respectively. The as-cut specimens were chemomechanically polished for damaged surface layer removal. The as-treated surface had no micro- or nanocracks and was leveled and smooth.

The cracking resistance (K_{1c}) was calculated using Niihara's formula for the Palmqvist crack system [25–27]:

$$K_{1c} = 0.035(L/a)^{-1/2}(CE/H)^{2/5}Ha^{1/2}C^{-1} \quad (1)$$

where K_{1c} is the stress intensity coefficient (MPa·m$^{1/2}$), L is the radial crack length (m), a is the indentation half-width (m), C is the constraint factor (=3), E is Young's modulus (Pa) and H is the microhardness (Pa).

For K_{1c} calculation, radial cracks around the indentation were taken—the length of which met the criterion ($0.25 \leq l/a \leq 2.5$) for Palmqvist cracks.

The anisotropy of the fracture toughness in the (100) plane of the crystals was measured by rotating the specimens around a fourth-order axis through 0 to 90 deg with a 22.5 deg step. Although the above fracture toughness measurement method has a number of restrictions, it is widely used for measuring the fracture toughness of ZrO_2-based ceramics; yet the anisotropy data are an estimation rather than an exact measurement.

3. Results and Discussion

The test crystals had the compositions $(ZrO_2)_{1-x}(Sm_2O_3)_x$ (where x = 0.032, 0.037 and 0.04) and were, additionally, doped with 0.5 mol.% CeO_2. Hereinafter, the crystals compositions will be denoted as 3.2Sm0.5CeSZ, 3.7Sm0.5CeSZ and 4.0Sm0.5CeSZ, respectively.

The as-grown $(ZrO_2)_{0.995-x}(Sm_2O_3)_x(CeO_2)_{0.005}$ single crystals had orange color due to Ce^{3+} ions, this color changing after air annealing. The orange/red color was caused by the wide absorption band near 460 nm originating from the 4f→5d transition of Ce^{3+} ions [28]. The presence of Ce^{3+} ions in the crystals was further confirmed by the X-ray

adsorption near-edge structure data (XANES). Figure 1 shows the XANES spectrum of the 4.0Sm0.5CeSZ crystal, exhibiting two clear absorption bands at 5732 and 5738 eV, corresponding to the Ce^{4+} ions, and a broadened absorption band at 5727 eV, corresponding to the Ce^{3+} ions [29]. The data suggest that the $(ZrO_2)_{0.995-x}(Sm_2O_3)_x(CeO_2)_{0.005}$ crystals contained both Ce^{4+} and Ce^{3+} ions. Furthermore, qualitative comparison between the shapes of the experimental XANES spectrum and that of the earlier-reported one [29] suggests that the content of Ce^{3+} ions in the $(ZrO_2)_{0.995-x}(Sm_2O_3)_x(CeO_2)_{0.005}$ crystals was low and that cerium cations were mainly present in the form of Ce^{4+}.

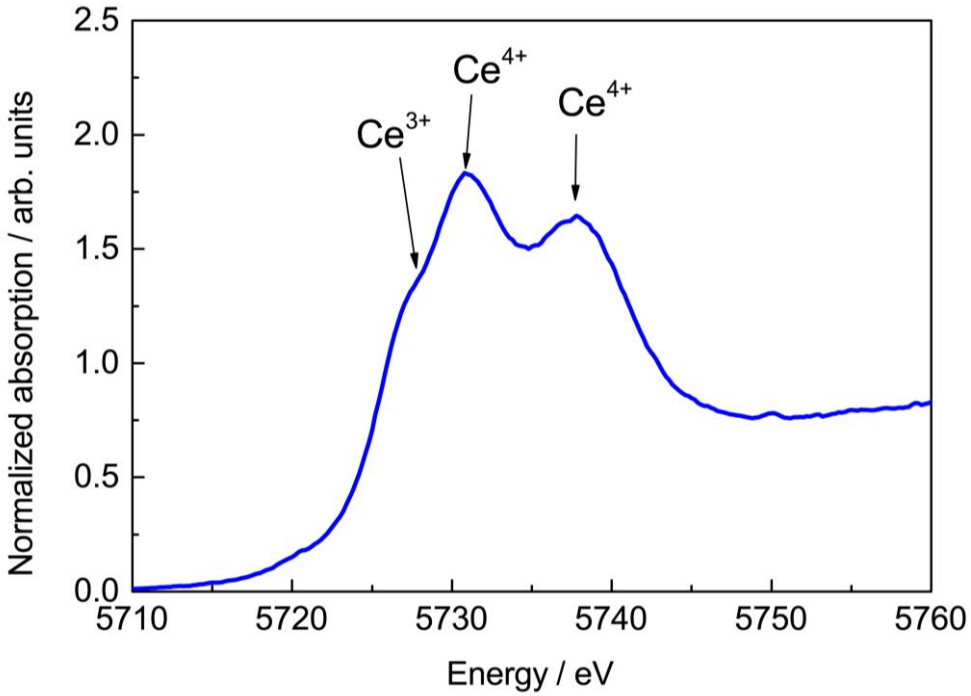

Figure 1. Ce ion XANES spectrum of 4.0Sm0.5CeSZ crystal.

X-ray phase data show that the 3.2Sm0.5CeSZ crystals contained a mixture of the monoclinic (m) and tetragonal (t) phases of zirconia. It should be noted that those crystals were visibly inhomogeneous in the bulk and had a few cracks. These macrodefects were probably caused by polymorphic transitions occurring during crystal cooling that were accompanied by volumetric changes. This phase composition was also typical of the 3.2SmSZ crystals that did not contain ceria [24]. Thus, ceria doping of crystals containing 3.2 mol.% stabilizing oxide did not stabilize the tetragonal phase in the whole bulk of the crystals. Other crystals contained only the tetragonal modifications (t and t′) of zirconia.

The cubic-to-tetragonal phase transition occurring during crystal cooling upon melt crystallization is a diffusion-free martensitic one and does not cause changes to the chemical composition of the material. The transition is mainly characterized by the migration speed of the phase boundary [15]. Further slow cooling of the crystals in the (c + t) two-phase field is accompanied by diffusive processes related to solid-solution decomposition in accordance with the phase diagram. Tetragonal-phase precipitates form in the bulk of the initial cubic solid solution. The precipitates are depleted of the stabilizing oxide in comparison with the initial composition (the t phase). The cubic phase is therefore enriched with the stabilizing oxide and undergoes a transition to the tetragonal phase to form a non-transformable t′ matrix.

As an example, Figure 2 shows a sample's diffractogram cut from a 4.0Sm0.5CeSZ crystal perpendicular to the <001> axis.

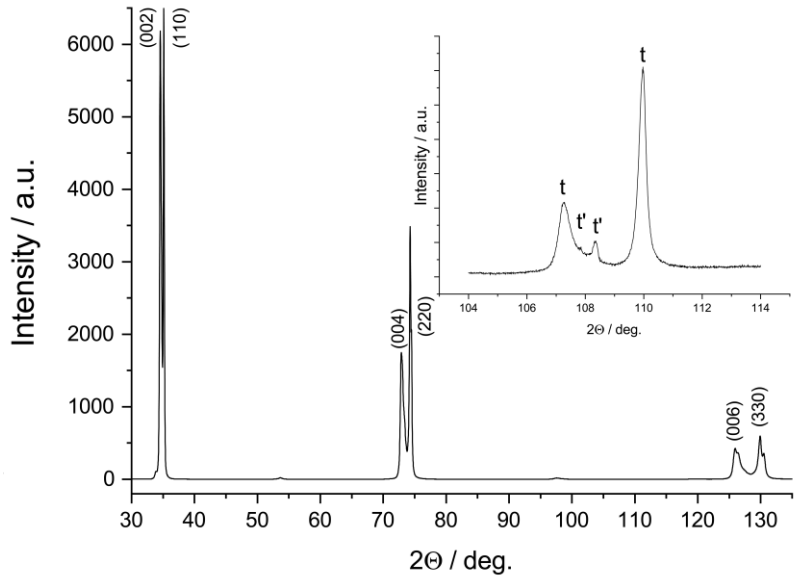

Figure 2. Diffraction pattern of 4.0Sm0.5CeSZ specimen cut from the crystal perpendicularly to the <001> direction.

Twinning in the crystals occurring in the (011) or (101) planes produced simultaneous different-order reflections from the (001) and (110) planes of the tetragonal ZrO_2 modification. In accordance with the $P4_2/mnc$ space group of the crystals, the diffraction pattern had the second-, fourth- and sixth-order reflections from the (001) plane and the first three order reflections from the (110) plane.

At high 2θ angles the diffraction patterns exhibited tetragonal phase splitting in two tetragonal phases with different lattice parameters. Some structural parameters of the tetragonal crystals are presented in Table 1. By way of comparison, Table 1 also shows earlier data for $(ZrO_2)_{1-x}(Sm_2O_3)_x$ crystals [24].

Table 1. Phase composition, lattice parameters and tetragonality degree of $(ZrO_2)_{0.995-x}(Sm_2O_3)_x(CeO_2)_{0.005}$ and $(ZrO_2)_{1-x}(Sm_2O_3)_x$ crystals.

Specimen	Phase	Content, wt.%	Lattice Parameters, Å	$c/\sqrt{2}a$
3.7SmSZ [24]	t	85 ± 5	a = 3.6062(2) c = 5.1866(2)	1.0170
	t′	15 ± 5	a = 3.6426(5) c = 5.1695(2)	1.0035
3.7Sm0.5CeSZ	t	90 ± 5	a = 3.6062(2) c = 5.1886(2)	1.0174
	t′	10 ± 5	a = 3.6426(5) c = 5.1682(2)	1.0032
4.0SmSZ [24]	t	75 ± 5	a = 3.6063(2); c = 5.1854(2)	1.0167
	t′	25 ± 5	a = 3.6429(5); c = 5.1692(2)	1.0034
4.0Sm0.5CeSZ	t	85 ± 5	a = 3.6063(1) c = 5.1877(2)	1.0172
	t′	15 ± 5	a = 3.6427(5) c = 5.1685(2)	1.0033

Analysis of the data in Table 1 shows that doping with 0.5 mol.% CeO_2 affected the lattice parameter c of the tetragonal phase the most effectively. For example, the lattice parameter c of the t phase grew from 5.1866 to 5.1886 Å for the 3.7SmSZ crystals and from 5.1854 to 5.1877 Å for the 4.0SmSZ ones. The lattice parameter c of the t′ phase decreased from 5.1695 to 5.1682Å for 3.7SmSZ and from 5.1692 to 5.1685 Å for 4.0SmSZ. Thus, CeO_2 doping increased the tetragonality degree of the transformable t phase and reduced the tetragonality of the non-transformable t′ phase. The tetragonality degree of zirconia-based tetragonal solid solutions is known to be directly related to the content of the stabilizing oxide [15]. Similar results were obtained for the Yb_2O_3-Nd_2O_3-ZrO_2 ceramics (1Yb–2Nd–

TZP), which also exhibited phase separation accompanied by a change in the tetragonality degree and, accordingly, stabilizing of oxide concentration in the tetragonal grains [30].

TEM study did not reveal differences between the structures of the $(ZrO_2)_{0.995-x}(Sm_2O_3)_x(CeO_2)_{0.005}$ and $(ZrO_2)_{1-x}(Sm_2O_3)_x$ crystals. Figure 3 shows a TEM image of the 3.7Sm0.5CeSZ crystal.

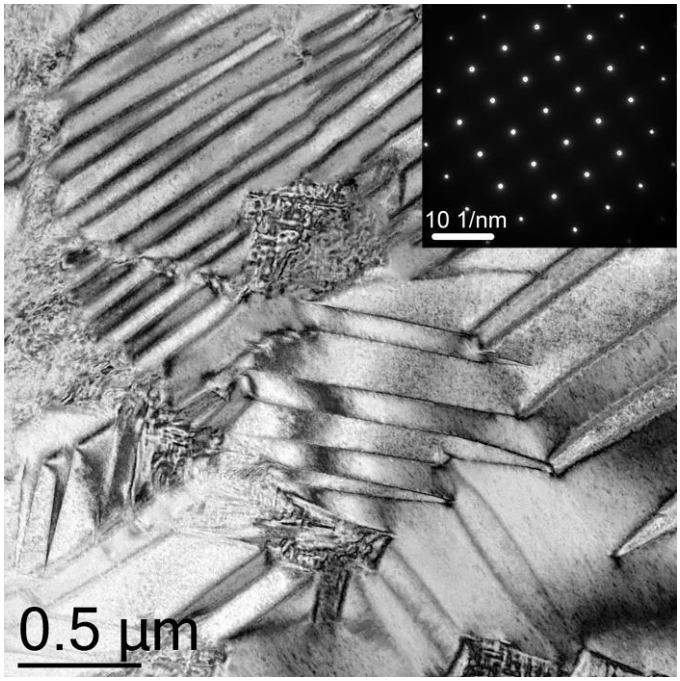

Figure 3. TEM image of 3.7Sm0.5CeSZ crystal.

The image (Figure 3) shows multiple twins. The image brightness at different sides of the twin boundary differs since lattice orientation changes upon crossing a coherent twin boundary. This structure is typical of all the test crystals. Despite the clearly expressed twinning structure of the crystals, the electron diffraction patterns do not contain typical additional reflections. For crystal twinning in the {110} plane the twin reflections coincide with the matrix reflections and cannot be resolved in the electron diffraction patterns at low tetragonality degrees. One can clearly see (Figure 3) two types of twin structures with different domain sizes in the crystals: a large-domain structure with typical domain sizes of 0.3–0.5 μm and a small-domain structure with typical domain sizes of < 0.1 μm located at the large-domain boundaries. The electron diffraction pattern for the region containing both fine and coarse twins is single-crystal. This fact suggests that differently sized structural features have similar orientations. The misorientation angles between regions with fine and coarse twins were within 2 deg. Similar structures were earlier observed in the $(ZrO_2)_{1-x}(Gd_2O_3)_x$ crystals. It was shown that the regions containing large twins were the t phase whereas the smaller twins pertained to the t′ phase. The Gd_2O_3 distribution between those phases proved to be inhomogeneous [31]. One can hypothesize that the inhomogeneous composition of the tetragonal solid solutions in the test crystals also changed the morphology of their twin structure, i.e., large domains pertained to the t phase, and small ones to the t′ phase.

The microhardness data for the crystals are summarized in Table 2. It can be seen that the two-phase 3.2Sm0.5CeSZ crystals containing the monoclinic phase had the lowest microhardness. CeO_2 doping of the crystals reduced their microhardness, but slightly, as compared to the $(ZrO_2)_{1-x}(Sm_2O_3)_x$ crystals. The tendency of microhardness growth with Sm_2O_3 concentration observed for the $(ZrO_2)_{1-x}(Sm_2O_3)_x$ crystals was also the case for the $(ZrO_2)_{0.995-x}(Sm_2O_3)_x(CeO_2)_{0.005}$ ones.

Table 2. Microhardness of $(ZrO_2)_{1-x}(Sm_2O_3)_x$ [24] and $(ZrO_2)_{0.995-x}(Sm_2O_3)_x(CeO_2)_{0.005}$ crystals.

Composition	Microhardness, GPa	Composition	Microhardness, GPa
3.2SmSZ	10.75 ± 0.30	3.2Sm0.5CeSZ	10.54 ± 0.25
3.7SmSZ	11.30 ± 0.30	3.7Sm0.5CeSZ	11.15 ± 0.25
4.0SmSZ	12.15 ± 0.30	4.0Sm0.5CeSZ	11.70 ± 0.25

Figure 4 shows the fracture toughness of the $(ZrO_2)_{0.995-x}(Sm_2O_3)_x(CeO_2)_{0.005}$ crystals as a function of indenter diagonal orientation relative to the crystallographic directions in the specimen plane. By way of comparison, Figure 4 shows the fracture toughness of the $(ZrO_2)_{1-x}(Sm_2O_3)_x$ crystals. The data clearly suggest that CeO_2 doping in all cases increased the fracture toughness of the crystals. The relatively low fracture toughness of the 3.2Sm0.5CeSZ crystals was probably caused by the presence of the monoclinic phase. Tetragonal crystals with high fracture toughness had the most expressed anisotropy. The 3.7Sm0.5CeSZ crystals had the highest fracture toughness of 16 MPa·$m^{1/2}$.

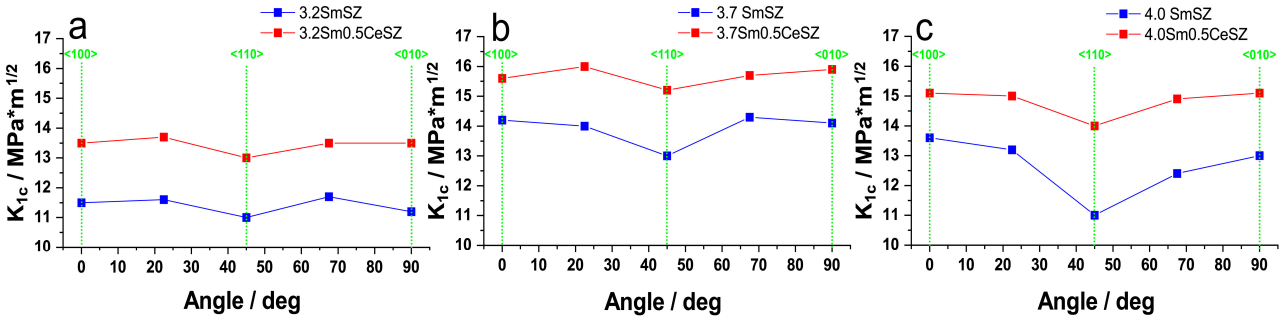

Figure 4. Fracture toughness of (**a**) 3.2Sm0.5CeSZ, (**b**) 3.7Sm0.5CeSZ and (**c**) 4.0Sm0.5CeSZ crystals depending on indenter diagonal orientation in {100} specimen plane. <100> direction corresponds to 0 arc deg.

It is well-known that the high fracture toughness of partially stabilized zirconia-based materials originates from the transformation strengthening mechanism. Theoretical analyses of the contribution from the transformation strengthening mechanism to the fracture toughness showed that contribution to be proportional to the content of the transformable tetragonal phase, its transformability and the transformation zone width [32]. Data on the transformation zone width and transformability of the tetragonal phase (R_m) (the relative quantity of the tetragonal phase that transformed to the monoclinic one) can be derived from local-phase analysis around the indentation. The transformability (R_m) was calculated from the monoclinic to tetragonal phase band intensity ratio in the Raman spectra using the following formula [33]:

$$R_m = \frac{I^m_{178} + I^m_{190}}{I^t_{146} + I^m_{178} + I^m_{190}} \quad (2)$$

where I^m_{178} and I^m_{190} are the intensities of the 178 and 190 cm^{-1} bands in the monoclinic phase spectrum, and I^t_{146} is the intensity of the 146 cm^{-1} band in the tetragonal phase spectrum. Figure 5 shows the transformation degrees at different points near the indentation for the 3.7Sm0.5CeSZ and 3.7SmSZ crystals.

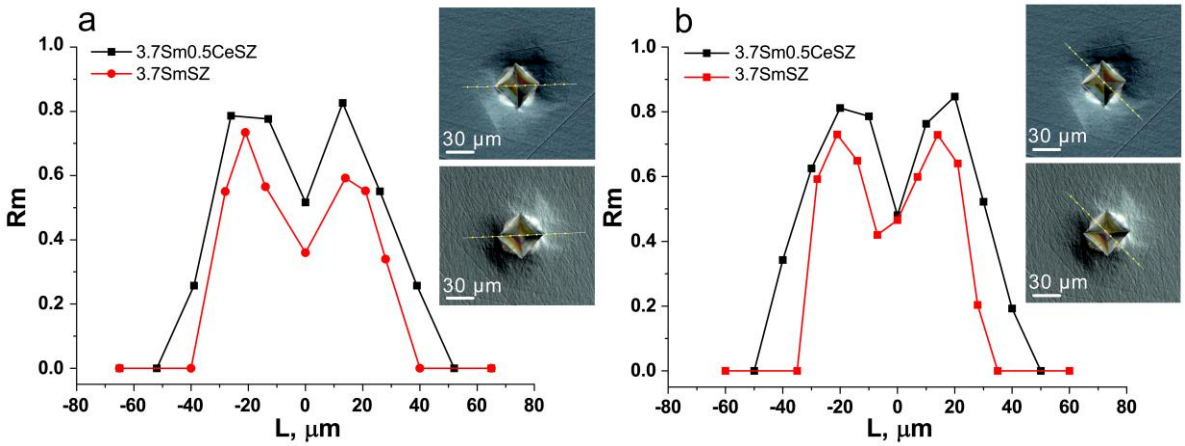

Figure 5. Degrees of tetragonal to monoclinic phase transformation for 3.7Sm0.5CeSZ and 3.7SmSZ crystals at local points near indentation for directions (**a**) along indenter diagonal and (**b**) along indenter side. Indentation boundaries are marked by dashes.

As can be seen from Figure 5, the region of the stress-induced t→m phase transition in the 3.7Sm0.5CeSZ crystals extended farther beyond the indentation boundaries than in the 3.7SmSZ crystals. The 3.7Sm0.5CeSZ crystals also exhibited a greater degree of transformation as compared to the 3.7SmSZ ones. Similar regularities were also observed for the 4.0Sm0.5CeSZ and 4.0SmSZ crystals. Thus, the addition of CeO_2 to solid solutions led to an increase in the intensity and expansion of the t→m phase-transformation region around the imprint during indentation. Both those factors increased the fracture toughness of the crystals.

Thus, analysis of the experimental data leads to the conclusion that CeO_2 doping of the $(ZrO_2)_{1-x}(Sm_2O_3)_x$ solid solutions increased the tetragonality degree of the transformable tetragonal t phase and the intensity of the indentation-induced tetragonal to monoclinic phase transition. All those factors eventually increased the fracture toughness of the CeO_2-doped $(ZrO_2)_{1-x}(Sm_2O_3)_x$ crystals.

The crystals were annealed in vacuum or in air at 1600 °C for 2 h.

Vacuum annealing changed the color of the crystals to black due to the formation of non-stoichiometric oxygen vacancies producing an intense absorption band in the visible spectrum. Annealing of the $(ZrO_2)_{0.995-x}(Sm_2O_3)_x(CeO_2)_{0.005}$ crystals, regardless of composition, either in air or in vacuum, caused visible changes to their surfaces. Figure 6 shows optical surface images of the crystals upon annealing in different environments.

The surfaces of the as-grown 3.7Sm0.5CeSZ and 4.0Sm0.5CeSZ crystals were smooth and homogeneous. The observed changes can be caused by a change in the phase composition of the crystals upon annealing.

X-ray diffraction phase composition analysis of the crystals showed that all the air- and vacuum-annealed test crystals contained only the monoclinic ZrO_2 modification. The general appearance of the as-annealed diffraction patterns for different compositions varied, but slightly. Figure 7 shows the diffraction pattern of the air-annealed 4.0Sm0.5CeSZ crystal.

The diffractogram (Figure 7) shows reflections of different orders from the {001} plane. A comparison of the angles between the planes with the tabular values for the monoclinic modification of ZrO_2 (space group $P2_1$) showed that a monoclinic phase was formed in all the studied samples after annealing.

Thus, study of the phase composition of the CeO_2-doped crystals showed that annealing produces (or increases the quantity of) the monoclinic phase. In our opinion, the formation of the monoclinic phase occurs spontaneously during crystal cooling after annealing at 1600 °C for 2 h.

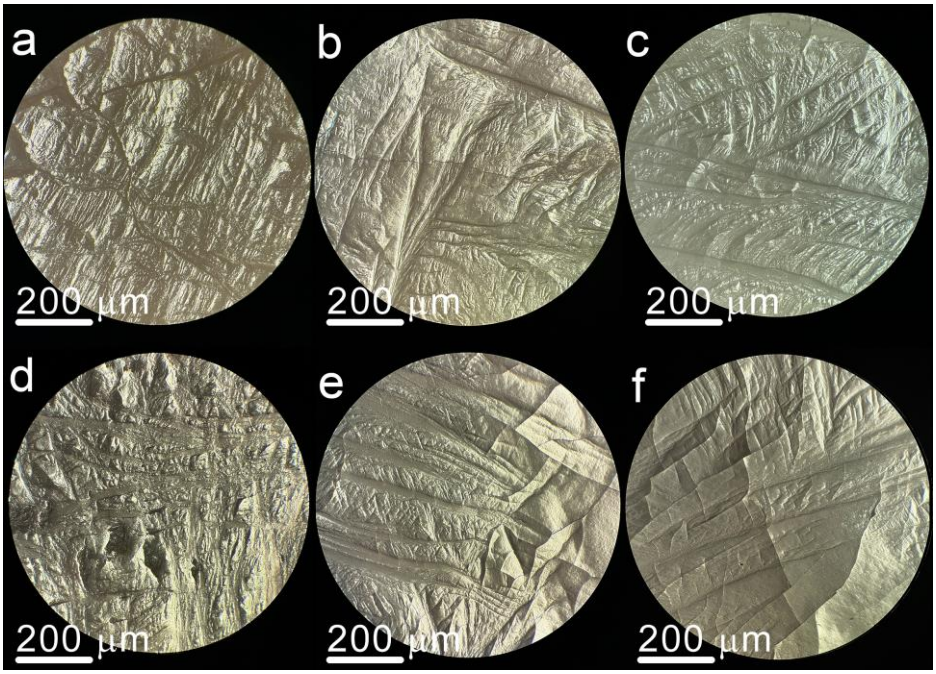

Figure 6. Surface images of (**a**,**d**) 3.2Sm0.5CeSZ, (**b**,**e**) 3.7Sm0.5CeSZ and (**c**,**f**) 4.0Sm0.5CeSZ crystals upon (**a**–**c**) air and (**d**–**f**) vacuum annealing.

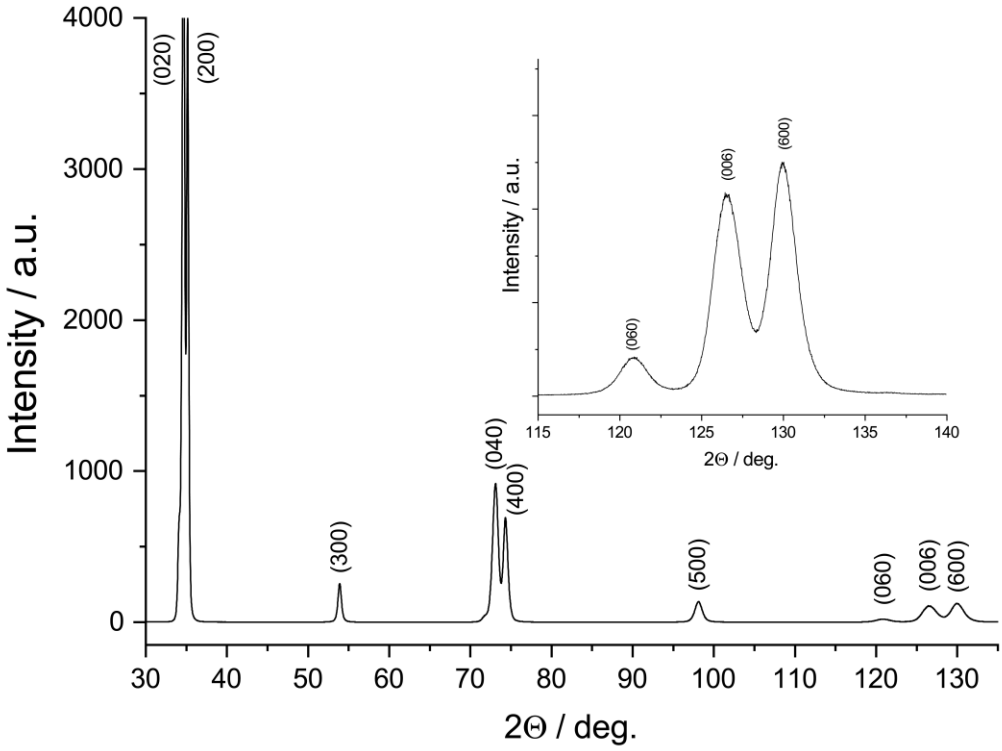

Figure 7. Diffraction pattern of air-annealed 4.0Sm0.5CeSZ crystal. The normal to the specimen plane is parallel to the <001> direction.

The observed changes in the phase composition of the crystals were accompanied by changes in their microhardness (Table 3).

Table 3. Microhardness of $(ZrO_2)_{0.995-x}(Sm_2O_3)_x(CeO_2)_{0.005}$ crystals before and after annealing in air and in vacuum.

Specimen	HV, GPa		
	As-Grown	Vacuum-Annealed	Air-Annealed
3.2Sm0.5CeSZ	10.54 ± 0.25	8.55 ± 0.30	8.50 ± 0.30
3.7Sm0.5CeSZ	11.15 ± 0.25	8.65 ± 0.30	8.60 ± 0.30
4.0Sm0.5CeSZ	11.70 ± 0.25	9.25 ± 0.30	8.70 ± 0.30

All the heat-treated crystals exhibited a decrease in the microhardness, probably due to the formation of, or an increase in, the quantity of the monoclinic phase in the crystal bulk upon annealing. The annealing environment had a negligible effect on the microhardness of the crystals.

High-temperature annealing had the greatest effect on the fracture toughness of the crystals. The as-annealed fracture toughness of the 3.2Sm0.5CeSZ, 3.7Sm0.5CeSZ and 4.0Sm0.5CeSZ crystals decreased dramatically, to within 2–3.5 MPa·$m^{1/2}$, the fracture toughness values exhibiting no anisotropy. Similar degradation of the structure and mechanical properties was earlier observed after annealing of 3.2SmSZ, 3.7SmSZ and 4.0SmSZ crystals [24].

Thus, CeO_2 doping of the $(ZrO_2)_{1-x}(Sm_2O_3)_x$ solid solutions in the experimental concentration range did not increase the high-temperature phase stability of the crystals and could not prevent high-temperature degradation of their fracture toughness.

4. Conclusions

The effect of ceria doping of $(ZrO2)_{1-x}(Sm_2O_3)_x$ solid solutions on their phase composition, microhardness and fracture toughness was studied. Doping with 0.5 mol.% CeO_2 increased the lattice parameter c of the transformable tetragonal t phase, and decreased the lattice parameter c of the non-transformable tetragonal t′ phase. At the same time, the tetragonality degree of the t phase increased while that of the t′ phase decreased. CeO_2 doping caused a more profound phase separation in the (c + t) two-phase region. As a result, the composition of the transformable t phase approached the t/(c + t) phase boundary, thus making the phase more transformable, whereas the composition of the non-transformable t′ phase shifted toward the (c + t)/c phase boundary.

CeO_2 doping had but little effect on the microhardness of the crystals but increased their fracture toughness as compared to the $(ZrO_2)_{1-x}(Sm_2O_3)_x$ ones. The 3.7Sm0.5CeSZ crystals had the highest fracture toughness, 16 MPa·$m^{1/2}$. That high fracture toughness was caused by an increase in the degree of the stress-induced tetragonal to monoclinic phase transition.

However, CeO_2 doping of the $(ZrO_2)_{1-x}(Sm_2O_3)_x$ solid solutions in the experimental concentration range did not increase the high-temperature phase stability of the crystals and did not prevent high-temperature degradation of their fracture toughness.

Author Contributions: Conceptualization, M.B., P.R., E.L. and N.T.; formal analysis, V.M., A.C., V.P., A.P., D.Z., D.K. and N.S.; investigation, N.T., N.S., A.P. and F.M.; methodology, P.R.; resources, M.B., A.K., E.L., V.M. and N.T.; supervision, M.B. and E.L.; validation, P.R. and N.T.; visualization, F.M.; writing—review and editing, M.B., N.T., E.L. and P.R. All authors have read and agreed to the published version of the manuscript.

Funding: This work was financially supported by the Moscow Polytechnic University within the framework of the grant named after Pyotr Kapitsa.

Data Availability Statement: The original contributions presented in the study are included in the article.

Conflicts of Interest: The authors declare no conflicts of interest.

References

1. Chevalier, J.; Gremillard, L.; Virkar, A.V.; Clarke, D.R. The tetragonal-monoclinic transformation in zirconia: Lessons learned and future trends. *J. Am. Ceram. Soc.* **2009**, *92*, 1901–1920. [CrossRef]
2. Hannink, R.H.J.; Kelly, P.M.; Muddle, B.C. Transformation toughening in zirconia-containing ceramics. *J. Am. Ceram. Soc.* **2000**, *83*, 461–487. [CrossRef]
3. Qi, B.; Liang, S.; Li, Y.; Zhou, C.; Yu, H.; Li, J. ZrO_2 Matrix Toughened Ceramic Material-Strength and Toughness. *Adv. Eng. Mater.* **2022**, *24*, 2101278. [CrossRef]
4. Hisbergues, M.; Vendeville, S.; Vendeville, P. Review zirconia. *J. Biomed. Mater. Res. B Appl. Biomater.* **2009**, *88B*, 519–529. [CrossRef]
5. Deng, Y.; Wang, C.; Xu, X.; Li, H. Machine learning potential for Ab Initio phase transitions of zirconia. *Theor. Appl. Mech. Lett.* **2023**, *13*, 100481. [CrossRef]
6. Heuer, A.H. Transformation Toughening in ZrO_2-Containing Ceramics. *J. Am. Ceram. Soc.* **1987**, *70*, 689–698. [CrossRef]
7. Song, X.; Ding, Y.; Zhang, J.; Jiang, C.; Liu, Z.; Lin, C.; Zheng, W.; Zeng, Y. Thermophysical and mechanical properties of cubic, tetragonal and monoclinic ZrO_2. *J. Mater. Res. Technol.* **2023**, *23*, 648–655. [CrossRef]
8. Cheng, J.; Tian, C.; Yang, J.; He, J. Electrical and mechanical properties of Sm_2O_3 doped Y-TZP electrolyte ceramics. *Ceram. Int.* **2018**, *44*, 17033–17037. [CrossRef]
9. Bejugama, S.; Chameettachal, S.; Pati, F.; Pandey, A.K. Tribology and in-vitro biological characterization of samaria doped ceria stabilized zirconia ceramics. *Ceram. Int.* **2021**, *47*, 17580–17588. [CrossRef]
10. Rauchs, G.; Fett, T.; Munz, D.; Oberacker, R. Tetragonal-to-monoclinic phase transformation in CeO2-stabilised zirconia under uniaxial loading. *J. Eur. Ceram. Soc.* **2001**, *21*, 2229–2241. [CrossRef]
11. Palmero, P.; Fornabaio, M.; Montanaro, L.; Reveron, H.; Esnouf, C.; Chevalier, J. Towards long lasting zirconia-based composites for dental implants: Part I: Innovative synthesis, microstructural characterization and invitro stability. *Biomaterials* **2015**, *50*, 38–46. [CrossRef]
12. Savin, A.; Craus, M.L.; Turchenko, V.; Bruma, A.; Dubos, P.A.; Malo, S.; Konstantinova, T.E.; Burkhovetsky, V.V. Monitoring techniques of cerium stabilized zirconia for medical prosthesis. *Appl. Sci.* **2015**, *5*, 1665. [CrossRef]
13. Reveron, H.; Fornabaio, M.; Palmero, P.; Fürderer, T.; Adolfsson, E.; Lughi, V.; Bonifacio, A.; Sergo, V.; Montanaro, L.; Chevalier, J. Towards long lasting zirconia-based composites for dental implants: Transformation induced plasticity and its consequence on ceramic reliability. *Acta Biomater.* **2017**, *48*, 423–432. [CrossRef] [PubMed]
14. Wang, C.; Zinkevich, M.; Aldinger, F. Phase diagrams and thermodynamics of rare-earth-doped zirconia ceramics. *Pure Appl. Chem.* **2007**, *79*, 1731–1753. [CrossRef]
15. Yoshimura, M.; Yashima, M.; Noma, T.; Sōmiya, S. Formation of diffusionlessly transformed tetragonal phases by rapid quenching of melts in ZrO_2-$RO_{1.5}$ systems (R = rare earths). *J. Mater. Sci.* **1990**, *25*, 2011–2016. [CrossRef]
16. Guo, L.; Li, M.; Zhang, C.; Huang, X.; Ye, F. Dy_2O_3 stabilized ZrO_2 as a toughening agent for $Gd_2Zr_2O_7$ ceramic. *Mater. Lett.* **2017**, *188*, 142–144. [CrossRef]
17. Chislov, A.S.; Borik, M.A.; Kulebyakin, A.V.; Lomonova, E.E.; Milovich, F.O.; Myzina, V.A.; Ryabochkina, P.A.; Sidorova, N.V.; Tabachkova, N.Y. Comparison of the structure and physicochemical properties of ZrO_2 based crystals partially stabilized with. Y_2O_3, Gd_2O_3 and Sm_2O_3. *Mod. Electron. Mater.* **2024**, *10*, 3–10. [CrossRef]
18. Zhu, W.; Nakashima, S.; Marin, E.; Gu, H.; Pezzotti, G. Annealing-induced off-stoichiometric and structural alterations in Ca^{2+}-and Y^{3+}-stabilized zirconia ceramics. *Materials* **2021**, *14*, 5555. [CrossRef]
19. Schulz, U. Phase transformation in EB-PVD yttria partially stabilized zirconia thermal barrier coatings during annealing. *J. Am. Ceram. Soc.* **2000**, *83*, 904–910. [CrossRef]
20. Cao, X.; Vassen, R.; Wang, J.; Zou, B.; Li, S.; Hui, Y.; Yuan, J.; Song, W.; Cao, Q.; Jiang, J.; et al. Degradation of zirconia in moisture. *Corros. Sci.* **2020**, *176*, 109038. [CrossRef]
21. Zhu, W.; Nakashima, S.; Marin, E.; Gu, H.; Pezzotti, G. Microscopic mapping of dopant content and its link to the structural and thermal stability of yttria-stabilized zirconia polycrystals. *J. Mater. Sci.* **2020**, *55*, 524–534. [CrossRef]
22. Turon-Vinas, M.; Roa, J.J.; Marro, F.G.; Anglada, M. Mechanical properties of 12Ce-ZrO_2/3Y-ZrO_2 composites. *Ceram. Int.* **2015**, *41*, 14988–14997. [CrossRef]
23. Borik, M.; Kulebyakin, V.; Myzina, V.; Lomonova, E.E.; Milovich, F.O.; Ryabochkina, P.A.; Sidorova, N.V.; Shulga, N.Y.; Tabachkova, N.Y. Mechanical characteristics, structure, and phase stability of tetragonal crystals of ZrO_2–Y_2O_3 solid solutions doped with cerium and neodymium oxides. *J. Phys. Chem. Solids* **2021**, *150*, 109808. [CrossRef]
24. Borik, M.; Chislov, A.; Kulebyakin, A.; Lomonova, E.E.; Milovich, F.O.; Myzina, V.; Ryabochkina, P.A.; Sidorova, N.V.; Tabachkova, N.Y. Phase Composition and Mechanical Properties of Sm_2O_3 Partially Stabilized Zirconia Crystals. *Crystals* **2022**, *12*, 1630. [CrossRef]
25. Niihara, K. A fracture mechanics analysis of indentation-induced Palmqvist crack in ceramics. *J. Mater. Sci. Lett.* **1983**, *2*, 221–223. [CrossRef]
26. Niihara, K.; Morena, R.; Hasselman, D.P.H. Evaluation of KIc of brittle solids by the indentation method with low crack-to-indent ratios. *J. Mater. Sci. Lett.* **1982**, *1*, 13–16. [CrossRef]
27. Moradkhani, A.; Baharvandi, H. Effects of additive amount, testing method, fabrication process and sintering temperature on the mechanical properties of Al2O3/3Y-TZP composites. *Eng. Fract. Mech.* **2018**, *191*, 446–460. [CrossRef]

28. Orera, V.M.; Merino, R.I.; Peña, F. $Ce^{3+} \leftrightarrow Ce^{4+}$ conversion in ceria-doped zirconia single crystals induced by oxido-reduction treatments. *Solid State Ion.* **1994**, *72 Pt 2*, 103002. [CrossRef]
29. Kozlova, A.P.; Kasimova, V.M.; Buzanov, O.A.; Chernenko, K.; Klementiev, K.; Pankratov, V. Luminescence and vacuum ultraviolet excitation spectroscopy of cerium doped $Gd_3Ga_3Al_2O_{12}$ single crystalline scintillators under synchrotron radiation excitations. *Results Phys.* **2020**, *16*, 103002. [CrossRef]
30. Kern, F. Ytterbia-neodymia-costabilized TZP-Breaking the limits of strength-toughness correlations for zirconia? *J. Eur. Ceram. Soc.* **2013**, *33*, 965–973. [CrossRef]
31. Borik, M.A.; Chislov, A.S.; Kulebyakin, A.V.; Lomonova, E.E.; Milovich, F.O.; Myzina, V.A.; Ryabochkina, P.A.; Sidorova, N.V.; Tabachkova, N.Y. Effect of heat treatment on the structure and mechanical properties of partially gadolinia-stabilized zirconia crystals. *J. Asian Ceram. Soc.* **2021**, *9*, 559–569. [CrossRef]
32. Evans, A.G.; Cannon, R.M. Overview no. 48. Toughening of brittle solids by martensitic transformations. *Acta Metall.* **1986**, *34*, 761–800. [CrossRef]
33. Chien, F.R.; Ubic, F.J.; Prakash, V.; Heuer, A.H. Stress-induced martensitic transformation and ferroelastic deformation adjacent microhardness indents in tetragonal zirconia single crystals. *Acta Mater.* **1998**, *46*, 2151–2171. [CrossRef]

The European Union's Horizon 2020 Framework Program H2020-WIDESPREAD-01-2016-2017-TeamingPhase2 under grant agreement No. 739508, project CAMART2.